Towards collapse and revival from first principles on a Qubit in a Storage Ring

José Gómez Aleixandre

Supervisor: Andreas Adelmann
Advisors: Sebastian Heinekamp, Raphael Husistein

December 30, 2025

Abstract

The possibility of employing crystalline ion beams in storage rings has been explored since the early 2000s [1, 2]. We build on the work of R. Husistein [3] and M. Solinas [4] towards an implementation of a simulation of the full quantum state. For this, we develop a method to entangle the external and internal states, including the interaction between them. This implementation was successfully tested on spin states, whereas coherent Rabi oscillations could not be observed for isospin states. We also address convergence issues and attempt to gain insight into why Rabi oscillations could not be demonstrated.

ETH
Eidgenössische Technische Hochschule Zürich
Swiss Federal Institute of Technology Zurich

PAUL SCHERRER INSTITUT
PSI

Contents

1 Theory and Methods

1.1 Motivation

In 2020, Brown & Roser [1] suggested the usage of storage rings as quantum computers. The qubits should consist of ions in a crystalline ion beam, a state of matter achieved successfully in 2001 [2]. By skillfully placing lasers along the ring, transitions between two hyperfine states can be driven, and hence two distinct quantum states can be resolved.

As Brown & Roser acknowledge, there are still a variety of experimental issues that need to be resolved, such as the cooling limitations of a storage ring beam compared to an ion trap, the synchronization of the quantum operations due to the continuous circulation of the beam, or the effective implementation of quantum gates. However, experiments suggest that both qubit preparation and readout can be performed with high fidelity. This suggests that numerical simulations could provide a reliable assessment of the viability of using a storage ring for quantum computations.

In an attempt to approach this question from first principles, R. Husistein [3] implemented algorithms for the simulation of both the electronic and phononic states of an ion, and showed by means of a toy example that entanglement between them could be achieved. Later, the work of M. Solinas [4] allowed for the introduction of spin and isospin degrees of freedom (DoFs) as well as for the generalization to interactions with time-varying electromagnetic (EM) fields. Building on their work, the aim of this project is to perform a simulation of the full state using a complete model, including all interactions of all DoFs with the EM fields and between the internal and external states[1].

1.2 Theoretical model

1.2.1 The Hamiltonian of the full state

The Hamiltonian that governs the time evolution of the full state $|\Psi\rangle = |\psi_{\text{int}}\rangle \otimes |\psi_{\text{ext}}\rangle$ can be written as

$$H = H_{\text{int}} + H_{\text{ext}} + H_{\text{I}} \,.$$

If we represent the full Hilbert space as $\mathcal{H} = \mathcal{H}_{\text{int}} \otimes \mathcal{H}_{\text{ext}}$, the Hamiltonian can be written in operator form as

$$\hat{H} = \hat{H}_{\text{int}} \otimes \mathbb{1}_{\text{ext}} + \mathbb{1}_{\text{int}} \otimes \hat{H}_{\text{ext}} + \hat{H}_{\text{I}} \,.$$

Hence, H_{int} and H_{ext} act only on the internal and external states, respectively, whereas the last term, representing the interaction between both, acts on the full state.

The term acting on the internal state is given by

$$H_{\text{int}} = \underbrace{\frac{p^2}{2m}}_{:=T} - \overbrace{\frac{Z}{\left|\vec{r}_{\text{el}} - \vec{R}_{\text{nuc}}\right|}}^{:=V_{\text{ECP}}} + \underbrace{\frac{\mu_{\text{B}}}{\hbar}\left(\vec{L} + g_S \vec{S}\right) \cdot \vec{B}(t) + \frac{\mu_{\text{N}}}{\hbar} g_I \vec{I} \cdot \vec{B}(t)}_{:=H_{\text{Z}}} + \overbrace{\eta \vec{L} \cdot \vec{S}}^{:=H_{\text{SO}}} + \underbrace{A_{\text{hfs}} \vec{I} \cdot \vec{J}}_{:=H_{\text{HF}}} + \overbrace{\vec{d} \cdot \vec{E}(t)}^{:=H_{\text{ED}}} \,, \tag{1}$$

and includes the kinetic term (T) , the potential term according to an effective core potential (ECP) model (V_{ECP}) , the Zeeman term (H_{Z}) , the spin-orbit interaction (H_{SO}) , the hyperfine interaction (H_{HF}) as well as the electric dipole interaction (H_{ED}) . While the Bohr and nuclear magnetons, as well as the electron g-factor, are well-known universal constants, it is worth noting that the nuclear g-factor (g_I) and the coupling constants of the spin-orbit and hyperfine interactions depend on the atom or molecule under consideration.

The term acting on the external state is modeled as

$$H_{\text{ext}} = -\frac{\epsilon^4}{2}\Delta_{\vec{r}} + V(\vec{r}) \,, \tag{2}$$

[1] From here on, the terms "external" and "phononic" states will be used interchangeably. Furthermore, the term "internal" state will refer to the electronic DoF together with the spin and isospin ones.

with the Laplace operator $\Delta_{\vec{r}}$ representing the kinetic term and $V(\vec{r})$ being a smooth real potential. This model can yield a solution to the time-dependent Schrödinger equation (TDSE) in any regime ranging from a fully classical ($\epsilon \to 0$) to a fully quantum ($\epsilon = 1$) case [5]. A common choice for $V(\vec{r})$ is a harmonic or parabolic potential, which can be represented as

$$V(\vec{r}) = \frac{1}{2}\left(\sigma_x x^2 + \sigma_y y^2 + \sigma_z z^2\right) \tag{3}$$

for some parameters $\sigma_{x,y,z}$. In an ion trap or storage ring, this choice of potential can be justified because true potentials can be very well approximated by Eq. (3) in the vicinity of the rest position of the ions, which are assumed not to be subject to large displacements.

To properly interpret the interaction term between the internal and external states, it is necessary to understand its physical nature. When the nucleus is at rest ($\vec{R}_{\text{nuc}} = \vec{R}_0$), the energy of the valence electrons is determined by the core Hamiltonian[2] (H_0). However, a displacement of the nucleus ($\vec{u} := \vec{R}_0 - \vec{R}_{\text{nuc}} \neq \vec{0}$) induces a change in the electronic energy which depends on the electronic distribution, i.e., on the state of the system. This is known as electron-phonon coupling and is dominantly a first-order effect in terms of the potential [6]. Thus, the interaction Hamiltonian can be modeled as

$$H_{\text{I}} = -\vec{u} \cdot \nabla_{\vec{R}} E_{\text{el}}\left(\vec{r}_{\text{el}}\right)\big|_{\vec{R}_0} . \tag{4}$$

1.2.2 The internal state

The internal state consists of the electronic state, which describes the valence electrons of the atom, the spin, and the isospin:

$$|\psi_{\text{int}}\rangle = |\psi_{\text{el}}\rangle \otimes |s\rangle \otimes |f\rangle .$$

While the spin and isospin parts are already represented by basis states, it is necessary to expand $|\psi_{\text{el}}\rangle$ on an appropriately chosen basis. For multiparticle atoms as well as in the context of computational molecular dynamics, a widespread and efficient choice is the Hartree-Fock (HF) theory framework, in which the full wavefunctions are represented using Slater determinants [7]. R. Husistein [3] showed that by choosing contracted Gaussian-type orbitals (CTGO) $|\chi_k\rangle$ as basis functions, the Roothaan equation can be solved with this method to find the energy and wavefunction of the atomic ground state. Then, he also demonstrated that the HF method can be extended to a real-time time-dependent HF method, which, by means of an explicit second-order trapezoidal Magnus propagator (E2TMP) algorithm, yields the time evolution of the wavefunction with high precision. Although several sets of CTGO bases exist, each has different characteristics and functionalities. Numerical experiments conducted by F. Welper [8] established that the cc-pvNz basis set offers precise results, although at a higher computational cost. These basis states fit the case treated here well, since they are valence-only but include core-valence correlations[3]. Therefore, the electronic state will be represented as

$$|\psi_{\text{el}}\rangle = \sum_{k=1}^{\mathcal{K}} a_k |\chi_k\rangle .$$

1.2.3 The external state

The external state represents the mechanical DoFs of the nucleus. It models its displacement from the rest position as mechanical excitations or phonons. It is common practice, in particular in the

[2] In the model from Eq. (1), this represents the kinetic and potential terms. For a concrete description of the numerical model of the core Hamiltonian under the Hartree-Fock theory, see [3].

[3] The acronym stands for correlation consistent polarized valence N zeta basis set. "Valence-only" means that they only consider the electrons in the valence shells, which are the relevant ones for calculations with ECP potential models.

context of harmonic potentials, to model this as a Fock state $|n\rangle$, or more generally as a coherent state

$$|\alpha\rangle = e^{-|\alpha|^2/2} \sum_{n=0}^{\infty} \frac{\alpha^n}{\sqrt{n!}} |n\rangle \ .$$

This description is often used to treat the mechanical DOFs of quantum systems that involve classical or semiclassical fields as well as time-resolved experiments. Fock states, and thus by extension, coherent states are energy eigenstates of the harmonic oscillator. Furthermore, coherent states allow for the representation of quantum states without a definite number of phonons; rather, the mechanical excitations follow a Poissonian distribution of phonon numbers. Hence, a coherent state is the perfect quantum analog of a classical harmonic oscillator [9, 10].

Since it is computationally impossible to use an infinite-dimensional basis, the external state will be represented by a truncated coherent state, i.e. ,

$$|\psi_{\text{ext}}\rangle = e^{-|\alpha|^2/2} \sum_{n=0}^{\mathcal{N}} \frac{\alpha^n}{\sqrt{n!}} |n\rangle =: \sum_{n=0}^{\mathcal{N}} b_n |n\rangle \ .$$

1.2.4 The full quantum state

The full quantum state, including all considered DoFs, reads as follows[4]:

$$|\Psi\rangle = |f\rangle \otimes |s\rangle \otimes |\psi_{\text{el}}\rangle \otimes |\psi_{\text{ext}}\rangle = \sum_{f=-I}^{I} \sum_{s\in\{\uparrow,\downarrow\}} \sum_{k=1}^{\mathcal{K}} \sum_{n=0}^{\mathcal{N}} c_{f,s,k,n} |f\rangle \otimes |s\rangle \otimes |\chi_k\rangle \otimes |n\rangle \ . \tag{5}$$

1.3 Numerical model

Since we are working in the Schrödinger picture[5], the time evolution of the full state can be tracked by considering the time evolution of the coefficients $c_{f,s,k,n}(t)$ in Eq. (5).

1.3.1 The data structure

When only considering the internal state, the preferred data structure for the bookkeeping of the coefficients during the time evolution was the density matrix, i.e. ,

$$\rho^{(\text{int})}_{f,g,s,r,k,l} := \tilde{a}_{f,s,k} \cdot \tilde{a}^{\star}_{g,r,l} \, .$$

This is mathematically the natural data structure, which also flows smoothly into the E2TMP algorithm that solves the Liouville-von Neumann equation for orthogonalized versions of the Fock operator and the density matrix[6]. Furthermore, M. Solinas [4] showed that this approach could be applied not only to the electronic state, but to the entire internal state, including the spin and isospin DoFs.

[4] The ordering of the Hilbert spaces in the tensor product is irrelevant. This choice corresponds to the data structure used for the time-evolution bookkeeping, as explained in Section 1.3.1.

[5] There might be operators that change in time because of their dependency on either time-varying fields or the state itself, but this approach is based on the assumption that the quantum state is what changes in time.

[6] The Fock operator is the operator appearing on the Roothaan equation. The necessary orthogonalization is due to the non-orthogonality of the basis of the electronic state $\{|\chi_k\rangle\}_{k\in\{1,\dots,\mathcal{K}\}}$. See [3] for a detailed explanation.

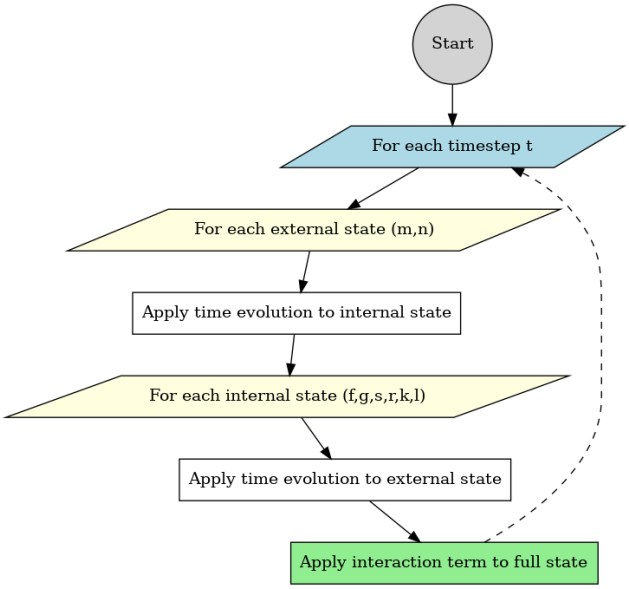

Figure 1: Workflow for each step of the time evolution when working with the data structure given by W.

To extend this isomorphically to the full state $|\Psi\rangle$, i.e., including the external state, we would need an operator analogous to the Fock operator, which would act with $H_{\text{int}} + H_{\text{ext}}$ on $\rho^{(\text{full})}$. Since the calculation of the corresponding matrix elements in a common basis is not available in the numerical tools at our disposal, the time evolution driven by H_{int} and H_{ext} must be performed separately. More specifically, using the properties of the tensor product, we can write[7]

$$\left(\hat{H}_{\text{el}} \otimes \mathbb{1}_{\text{ext}}\right)\left(\sum_{k=1}^{\mathcal{K}}\sum_{n=0}^{\mathcal{N}} |\chi_k\rangle \otimes |n\rangle\right) = \sum_{n=0}^{\mathcal{N}}\left[\left(\sum_{k=0}^{\mathcal{K}} \hat{H}_{\text{el}}\,|\chi_k\rangle\right) \otimes |n\rangle\right],$$

and analogously for the time evolution of the external state. The workflow that describes this process is shown in Fig. 1. Although this is possible to implement while working with a two-dimensional tensor such as $\rho^{(\text{full})}$, another structure might offer computational advantages as well as more simplicity. We propose[8] to store the coefficients $c_{f,s,k,n}(t)$ in a four-dimensional tensor W of shape $(d_I, d_I, 2, 2, \mathcal{K}, \mathcal{K}, \mathcal{N}, \mathcal{N})$, where d_I is the number of isospin projections of the atom. In this form,

$$W^{(t)}[f,g,s,r,k,l,n,m] = c_{f,s,k,n}(t) \cdot c^{\star}_{g,r,l,m}(t) =: w_{f,g,s,r,k,l,n,m}(t)$$

still holds, while

(a) the external state's partial density matrix is already traced out in the last two dimensions for each tuple (f,g,s,r,k,l), and

(b) the partial density matrix of the internal state $\rho^{(\text{int})}_{n,m}(t)$ for each tuple (n,m) can easily be obtained by properly reshaping $W^{(t)}[:,:,:,:,:,:,n,m]$.

Another advantage of this structure is the calculation of the relevant state populations: in both the case of spin state (i.e., when not considering the isospin DoF) and hyperfine state populations, it boils down to simple tracing-out operations (cf. Appendix A).

1.3.2 Time evolution of the internal state

As introduced in Sec. 1.2.2, the time evolution of the internal state is performed with the E2TMP algorithm, which solves the Liouville-von Neumann equation for H_{int} and $\rho^{(\text{int})}$. In order to obtain

[7] This is a simplified illustration of the idea that includes only the electronic and phononic states.

[8] Note that the extension of this approach to a system with fewer degrees of freedom (e.g., without considering the isospin) is trivial and does not change the process, only the dimensionality.

the corresponding unitary, the matrix elements of H_{int} with respect to the internal basis must be obtained. While the matrix elements involving the spin or isospin bases are well known from basic quantum mechanics theory, the terms affecting the electronic basis can be obtained straightforwardly from the quantum chemistry package PySCF, which includes all relevant integrals. For a detailed description of how H_{int} is evaluated with respect to the full basis of the internal state, see [4].

Although the time evolution according to the E2TMP algorithm should be unitary, some phase mixing or trace loss might occur due to floating-point precision issues. These can be mitigated by performing the following operations on $\rho^{(\text{int})}$ after each time step:

$$\rho^{(\text{int})} \mapsto \frac{1}{2}\left(\rho^{(\text{int})} + \rho^{(\text{int})\dagger}\right),$$
$$\rho^{(\text{int})} \mapsto \frac{1}{\text{tr}\left\{\rho^{(\text{int})}\right\}}\rho^{(\text{int})}.$$

Whereas the first correction is made to ensure hermiticity, the second one warrants that the state follows a "no-jump" phase-space trajectory, i.e. , that our observables remain in the subspace where the original state lived [11].

1.3.3 Time evolution of the external state

Gradinaru & Hagedorn [5] showed that the TDSE with respect to the Hamiltonian in Eq. (2) can be efficiently solved by projecting the corresponding quantum state onto Hagedorn wavepackets (HWPs), and they implemented their algorithm in the WaveBlockND package. For our purpose, this is an ideal solution, since HWPs are an optimal representation of a harmonic oscillator for several reasons: they form an invariant family under a purely quadratic Hamiltonian evolution, and they ensure minimal representation, since a single HWP can represent any pure Fock state.

Unfortunately, this algorithm, as implemented in the WaveBlockND package, only accepts quantum state coefficients and not density matrices, i.e. , it takes $c_{f,s,k,n}(t)$ rather than $w_{f,g,s,r,k,l,n,m}(t)$ as input. Although going back and forth between both representations can be easily achieved with eigendecomposition methods, these unnecessarily increase the computational cost and introduce a source of numerical errors.

Here, we present an alternative approach. First, consider a Fock state with n excitations $|n\rangle$ representing a three-dimensional harmonic oscillator. It is

$$|n\rangle = |n_x, n_y, n_z\rangle \qquad \text{with} \qquad n_x + n_y + n_z = n\,.$$

Therefore, any combination of $n_{x,y,z}$ that fulfills the last equation describes a harmonic oscillator with n excitations. Thus, we have

$$|n\rangle = \frac{1}{\sqrt{|\mathcal{S}|}} \sum_{n_x+n_y+n_z=n} |n_x, n_y, n_z\rangle\,, \tag{6}$$

where $\sqrt{|\mathcal{S}|}$ is a normalization constant that ensures $|\langle n|n\rangle|^2 = 1$. In particular, $|\mathcal{S}|$ is given by the number of terms in the sum above. Let $\hat{G}$ be the operator acting on $|n\rangle$, as implemented in WaveBlockND, that performs a timestep evolution of length Δt, and consider the full state for a fixed choice of (f, s, k)

$$|\Psi\rangle_{f,s,k} = \psi_{\text{int}}(f, s, k) \otimes \sum_{n=0}^{\mathcal{N}} c_{f,s,k,n}\,|n\rangle\,.$$

Then, for one timestep of length Δt, we have[9]

$$|\Psi'\rangle_{f,s,k} := \left(\mathbb{1} \otimes \hat{G}\right) |\Psi\rangle_{f,s,k} = \psi_{\text{int}}(f,s,k) \otimes \hat{G}\left(\sum_{n=0}^{\mathcal{N}} c_{f,s,k,n} |n\rangle\right) = \psi_{\text{int}}(f,s,k) \otimes \sum_{n=0}^{\mathcal{N}} c_{f,s,k,n} \hat{G} |n\rangle$$
$$= \psi_{\text{int}}(f,s,k) \otimes \sum_{n=0}^{\mathcal{N}} c_{f,s,k,n} |n'\rangle = \psi_{\text{int}}(f,s,k) \otimes \sum_{n=0}^{\mathcal{N}} c_{f,s,k,n} \sum_{\eta=0}^{\mathcal{N}} \epsilon_{n,\eta} |\eta\rangle \ . \tag{7}$$

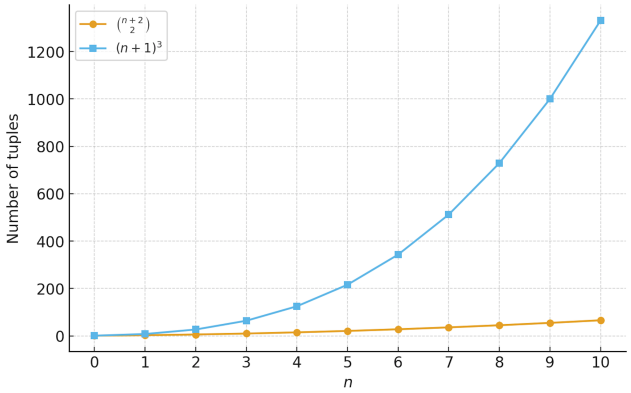

Figure 2: Comparison of the number of states that fulfill Eq. (6) to those used by the algorithm in the WaveBlockND package as a function of the number of excitations n.

Define the matrix $\tilde{U}_{\text{ext}}$ such that $\tilde{U}_{\text{ext}}[a,b] =: \tilde{\epsilon}_{ab}$. This matrix should be unitary, but due to the algorithm developed by Gradinaru & Hagedorn [5], the calculation represented by Eq. (7) might suffer from "norm leakage". In order to represent a three-dimensional HWP with n excitations, the algorithm uses a basis[10] ranging from $|0,0,0\rangle$ to $|n,n,n\rangle$. As can be seen in Fig. 2, the number of states that fulfill Eq. (6),

$$\binom{n+2}{2},$$

grows much more slowly than the number of basis states used by the algorithm, $(n+1)^3$. This means that the operator $\hat{G}$ might project the input state into basis states that are not considered in the expansion of $|n\rangle$, thus resulting in a norm loss. As a method for conserving the norm, we suggest using polar decomposition, i.e., to approximate $\tilde{U}_{\text{ext}}$ to its closest unitary in the sense of the Frobenius norm [12, 13]:

$$U_{\text{ext}} = \min_{Q,\text{unitary}} \left\| \tilde{U}_{\text{ext}} - Q \right\|_{\text{Fr}} = \mathcal{X}\mathcal{Y}^\dagger \ ,$$

where $\tilde{U}_{\text{ext}} = \mathcal{X}\Sigma\mathcal{Y}^\dagger$ is the singular value decomposition of $\tilde{U}_{\text{ext}}$.

Finally, if $\rho^{(\text{ext})}_{f,g,s,r,k,l}$ is the partial density matrix of the external state for a fixed tuple (f,g,s,r,k,l), its time evolution is given by

$$\rho^{(\text{ext})}_{f,g,s,r,k,l}(t+\Delta t) = U^\dagger_{\text{ext}} \, \rho^{(\text{ext})}_{f,g,s,r,k,l}(t) U_{\text{ext}} \ .$$

1.3.4 Time evolution due to the interaction term

The model presented in Eq. (4) for the interaction term is used recurrently to describe first-order electron-phonon coupling. It can be found in many fields of physics, from quantum optics in the

[9] For details on the calculation of $\epsilon_{n,\eta}$, cf. Appendix B.

[10] To use this algorithm, the user must choose a basis shape, which determines the basis states that will be employed. As R. Husistein showed [3], an efficient choice is the so-called hyperbolic cut shape, which includes all the states as described here.

context of excitons or polarons [14, 15], to condensed matter physics, where it is known as a Holstein-type coupling [16–18]. In the quantum chemistry literature, it appears as well and is known as linear vibronic coupling [19]. However, this model fails to describe the type of coupling considered here in a symmetrical single-ion system. In that case, and according to the Hellmann-Feynman theorem [20], the first-order change in the electronic energy should vanish.

In order to overcome this caveat, we propose the following approach. Contrary to the other two terms in the full Hamiltonian, the interaction Hamiltonian acts on the entire Hilbert space. However, it can be shown that this operator can be written in decomposable form, i.e., as the tensor product of two operators such that each one acts on a different subspace [16]:

$$\hat{H}_\mathrm{I} = \hat{F} \otimes \hat{X} \,.$$

On the one hand, we model $\hat{F}$ as the expectation value of the electronic energy with respect to the internal state basis, which can be efficiently calculated with the PySCF functionalities:

$$\hat{F} \coloneqq \left\langle \chi_i \middle| \left.\frac{\partial H_0}{\partial \vec{u}}\right|_{\vec{R}_0} \middle| \chi_j \right\rangle \,.$$

Note that this does not contradict the previous statement: the diagonal elements of $\hat{F}$ are zero, because they represent the vanishing first-order change in the electronic energy, but the non-diagonal ones are non-zero and describe the exchange of energy between the basis states $|\chi_i\rangle$ due to the electron-phonon coupling.

On the other hand, the term acting on the phononic space is modeled as

$$\hat{X} = \frac{1}{2} k \hat{u}^2 \,,$$

since the first-order coupling strength is, as argued above, zero[11]. Noting that

$$\hat{u} = \sqrt{\frac{1}{2M\omega}} \left(\hat{a} + \hat{a}^\dagger\right) \,,$$

with M is the mass of the nucleus, and ω the angular frequency of the interaction, we obtain

$$\hat{X} = \frac{\hbar\omega}{4} \left(\hat{a} + \hat{a}^\dagger\right)^2 \,.$$

Thereby, we used the relation [21, 22]

$$\omega = \sqrt{\frac{k}{M}} \,.$$

Furthermore, when calculating the expectation values of the ladder operators with respect to the Fock basis, we assume that a single interaction process between the internal and external states can only couple neighboring excitation manifolds, i.e., that a phonon state $|n\rangle$ can only couple to the states $|n \pm 1\rangle$. This assumption is reasonable as long as the system is not in a strongly nonlinear regime, which, for our case, can also be expected [23, 24].

Finally, in a similar way to the product basis, the full matrix representing $\hat{H}_\mathrm{I}$ can be constructed as the Kronecker product of the matrix representations of $\hat{F}$ and $\hat{X}$ with respect to the corresponding bases.

Since the interaction term is independent of spin and isospin, the interaction Hamiltonian will be block-diagonal with respect to these. By calculating the corresponding unitary matrix U_I and reshaping W into a density matrix form, the time evolution can be applied as follows:

$$\rho^{(\text{int-ext})}_{f,f,s,s}(t + \Delta t) = U_\mathrm{I}\, \rho^{(\text{int-ext})}_{f,f,s,s}(t)\, U_\mathrm{I}^\dagger \qquad \text{with} \qquad U_\mathrm{I} = e^{-iH_\mathrm{I}\Delta t} \,.$$

Note that in this case, too, issues with the unitarity might arise in the numerical implementation of U_I. To address them, both methods presented above in Sections 1.3.2 and 1.3.3 might be used.

[11] Cf. Appendix C for a detailed description on how to calculate the second-order coupling constant k, as well as for numerical estimations in the case of the $^9\mathrm{Be}^+$ ion.

2 Results and Discussion

In this section, the numerical simulations performed to evaluate our model are described, and plots of the obtained raw data are shown. At the same time, the results obtained are discussed. All plots of individual simulations follow the same structure. The upper subplot shows the difference between the total energy of the internal state[12] at time t and its initial value as a function of time. The lower subplot shows the time evolution of the trace of the full state as well as of the considered state populations (i.e., either the spin or hyperfine states). Additionally, boolean information about the electric and magnetic fields is also displayed in the lower subplot.

2.1 Electron-phonon interaction

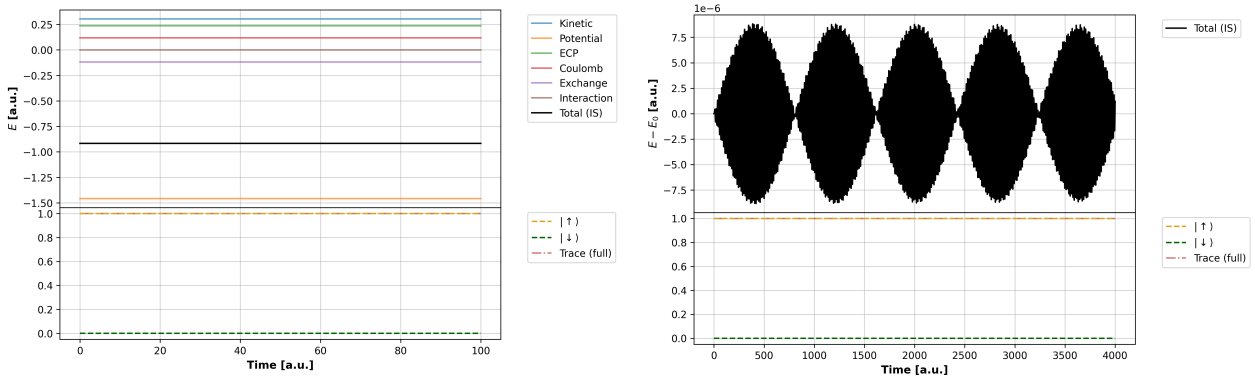

(a) **(b)**

Figure 3: **(a)** Baseline plot, where external and internal states are simulated without taking into account the interaction between them. **(b)** Simulation of the internal and internal states, including the interaction term. In both cases, no external fields were applied, and the isospin DoF was not included.

Figures 3a and 3b show the baseline plot and the effect of including the interaction term, respectively. In both cases, as well as in all other tests described in Sections 2.1 and 2.2, the isospin DoF was not included. These simulations were performed with values of $\mathcal{N} = 5$ and $\Delta t = 0.1$ a.u., and the system behaved as expected. Without external fields and without the interaction term, not only the total energy but also every one of its components is constant. Similarly, the initial populations of the system remain unchanged. The addition of the interaction term between the electronic and the phononic state induces an oscillatory exchange of energy between both. Since the accuracy with which the truncated Fock basis represents the external state depends on the cutoff value $\mathcal{N}$, the influence of this parameter on the amplitude of the oscillations was studied as well. As shown in Fig. 4, the amplitude of the energy oscillations converges towards a value of approximately

$$1.232 \cdot 10^{-5} \text{ Hartree} \approx 5.383 \cdot 10^{-23} \text{ J} \approx 0.336 \text{ meV}$$

for increasing $\mathcal{N}$. Electron-phonon interaction studies are generally done for solid-state lattices or in relation to vibrational effects in molecules [25]. Hence, it would be challenging to find reference values for this amplitude in the literature. Under the Born–Oppenheimer approximation, which is often assumed when treating electron-phonon interactions, non-adiabatic energy exchanges between electrons and phonons scale parametrically with the electron-to-nucleus mass ratio [26]. As a consequence, non-adiabatic corrections are strongly suppressed, and it is therefore valid to assume that

[12] Note that only the energy of the internal state has been tracked in these simulations. This is due to technical aspects of the package used to model the external state, which neither offers any possibility of obtaining the matrix form of the external state Hamiltonian in terms of Fock states nor can it calculate energies at different time steps from the state coefficients in the form that we track them. In the context of this investigation, from here on, the term "energy" will refer to energy of the internal state, and energy conservation will be assumed whenever the energy difference with respect to the initial value does not drift significantly in the long term.

the amplitude of the energy oscillations here observed should be of the same order of magnitude as the ratio of the masses between the valence electron and the nucleus. In the case of a single ion such as $^9BE^+$, the main sources of electronic-phononic exchange are recoil and zero-point motion associated with electronic binding [27]. A conservative estimation for this type of interaction yields a range of 0.1–1 meV , making the simulated energy exchange physically plausible.

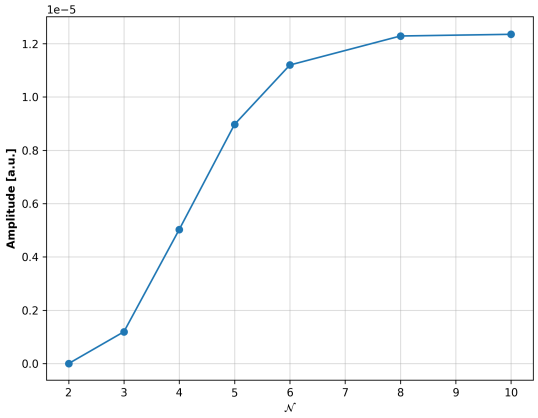

Figure 4: Convergence of the amplitude of the energy oscillations as a function of the truncation index $\mathcal{N}$ of the Fock basis.

2.2 Spin states

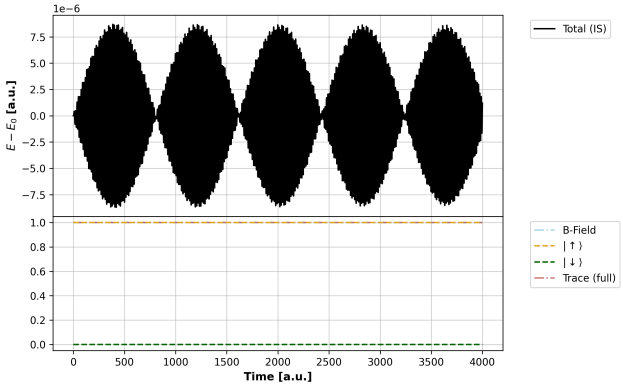

Figure 5: Effect of a constant magnetic field parallel to the spin polarization $\left(\vec{B} = B_z\right)$.

With these tests, we aim to show the effects of applying a constant magnetic on the system, while still not considering the isospin DoF. As can be seen by comparing Figs. 5 and 3b, a magnetic field along the z-direction, i.e., parallel to the polarization direction of the ion's spin, does not affect the dynamics of the system beyond a constant shift of the energy. However, when the field is polarized perpendicularly to the spin, the population between the spin states oscillates back and forth (Fig. 6a). This is known as Larmor precession, and its oscillation frequency depends linearly on the strength of the applied magnetic field (Fig. 6b) according to

$$\omega_{\text{Larmor}} = \left\| \gamma \vec{B} \right\| ,$$

where γ is the gyromagnetic ratio. Note that the system's dynamics also remain unchanged when choosing either perpendicular axis with respect to the spin polarization. The sole variation is an overall phase difference, which is not physically measurable. Figure 6a also shows that a perpendicularly polarized magnetic field induces an energy drift. By repeating this simulation for several

values of $\|\vec{B}\|$, we could show that this drift, which reduces the total energy of the internal state, depends quadratically on the magnetic field strength (Fig. 7).

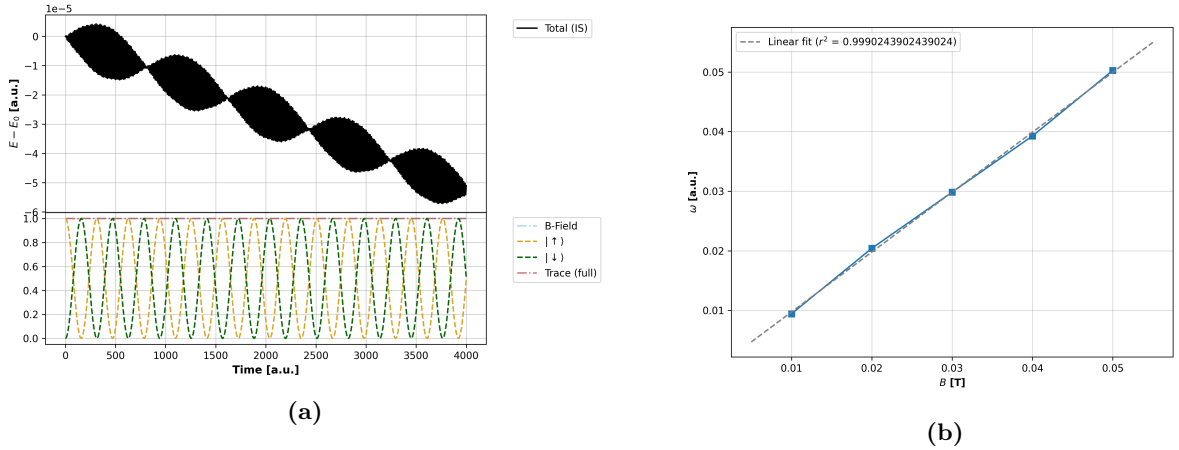

(a) **(b)**

Figure 6: **(a)** Larmor precession observed when applying a magnetic field perpendicular to the spin polarization. In this case, the magnetic field was polarized along the y-direction. **(b)** Dependence of the frequency of the Larmor precession on the magnetic field strength.

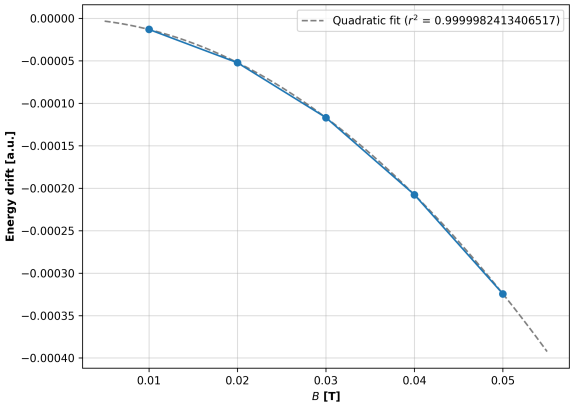

Figure 7: Drift of the total energy of the internal state due to an external magnetic field perpendicular to the spin polarization.

To determine the source of such drift, we investigated various simulation parameters. First, the effect of the Fock basis cutoff $\mathcal{N}$ was tested (Fig. 8). For constant values of $B = 0.01$ T and $\Delta t = 0.1$ a.u., the cutoff was modified, and the drift in the energy was tracked. Convergence can be observed for increasing $\mathcal{N}$, with stable values for $\mathcal{N} \gtrsim 8$. Since $|\psi\rangle_{\text{ext}}$ is modeled as a coherent state with $|alpha| = 1$, the phonon number follows a Poissonian distribution with unity mean and variance. Hence, by choosing [28]

$$\mathcal{N} \geq |\alpha|^2 + 6|\alpha| = 7\,,$$

which corresponds to a 6σ range around the mean, we can ensure that the probability for the true coherent state of being fully represented by the truncated one is given by

$$1 - \epsilon_{\text{trunc}} = 1 - \sum_{n=8}^{\infty} \mathcal{P}(n) = 1 - \sum_{n=8}^{\infty} \frac{e^{-1}}{n!} \approx 10^{-5}\,.$$

Therefore, for $\mathcal{N} > 7$, convergence to a high degree of accuracy should be expected, thus agreeing with our results above.

After this, the consequences of varying the duration of the time step were analyzed (Fig. 9). We observed convergence of both the oscillation amplitude and the energy drift for decreasing time step duration, with stable values for $\Delta t \leq 0.05$ a.u. This result agrees with that of Fig. 8. The simulations performed to obtain Fig. 8 were carried out with values of $\Delta t = 0.1$ a.u., and for the tests corresponding to Fig. 9, the cutoff value of the Fock basis was set to $\mathcal{N} = 5$. Comparing the corresponding data points in both plots, it can be easily seen that they are in agreement. Note that for obtaining the individual data points in Figs. 7, 8 and 9b, the energy difference $\Delta E := E - E_0$ as a function of time was fitted to a linear model, and the slope as well as the corresponding standard error estimation were extracted from the fit and plotted here.

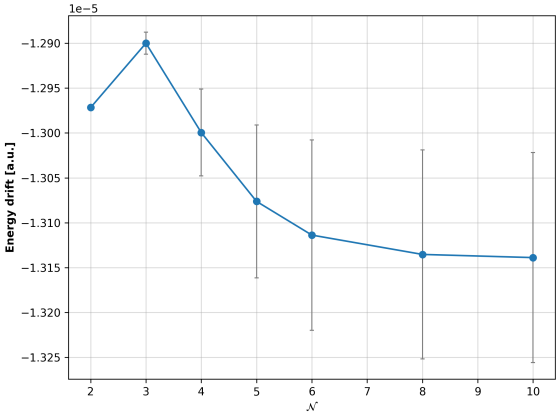

Figure 8: Drift of the total energy of the internal state as a function of the Fock basis cutoff parameter $\mathcal{N}$.

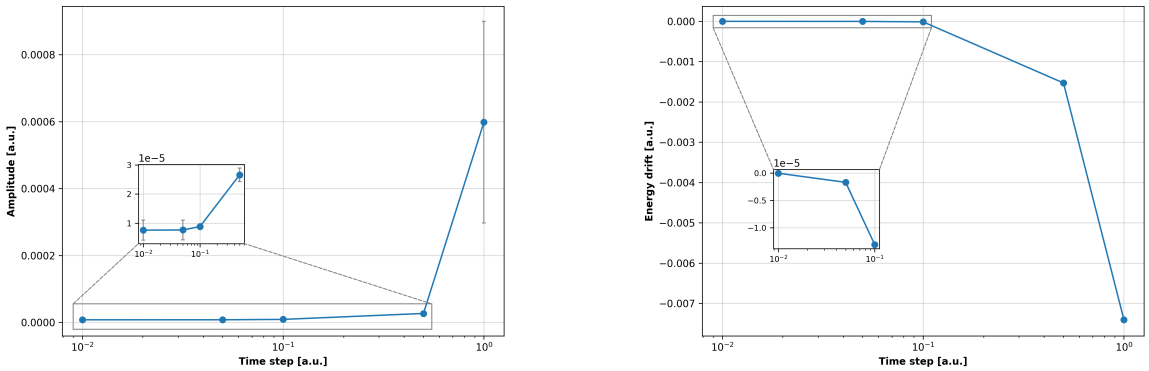

(a) **(b)**

Figure 9: **(a)** Amplitude of the energy oscillations as a function of the time step duration. **(b)** Energy drift as a function of the time step duration. Both plots were generated from simulations with a fixed magnetic field strength of $B = 0.01$ T.

Finally, we wanted to study the tradeoff between the accuracy obtained by decreasing the duration of the time step or increasing the cutoff $\mathcal{N}$ and the physical time required to compute one simulation step. This is displayed in Fig. 10, where it can be seen that the computational time increases linearly with the duration of the time step, while larger cutoff values result in a quadratic increase of the time needed to compute one simulation step.

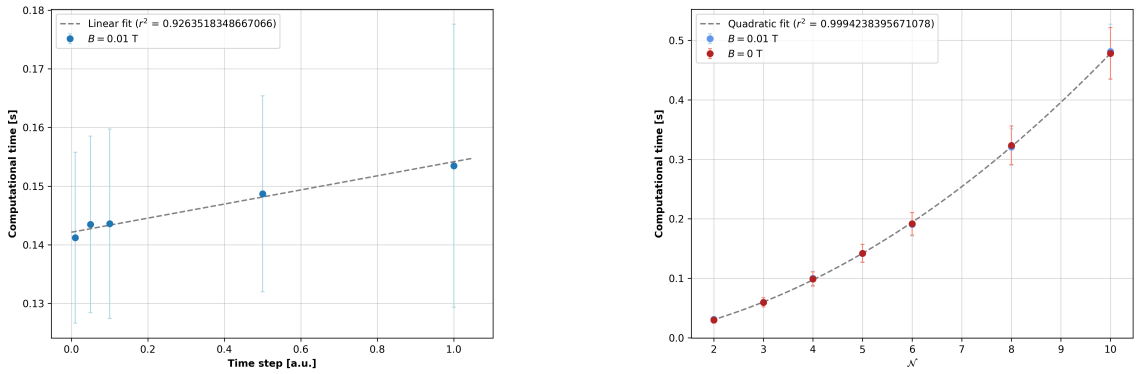

(a) **(b)**

Figure 10: Computational time per simulation step as a function of **(a)** the duration of the time step and **(b)** the cutoff value $\mathcal{N}$ of the Fock basis.

2.3 Isospin states

The final step of our study was to include the isospin DoF in the simulated system. In the absence of external fields, the observed behavior is expected to be the same as before. Figure 11b shows that for values of $\Delta t \geq 0.05$ a.u. , the system behaves unphysically. Even for $\Delta t = 0.01$ a.u. , a value that ensured convergence in the previous tests, still results in a slight upward drift in the energy (Fig. 11a). This indicates that simulating the full state is much more sensitive to the choice of time step duration.

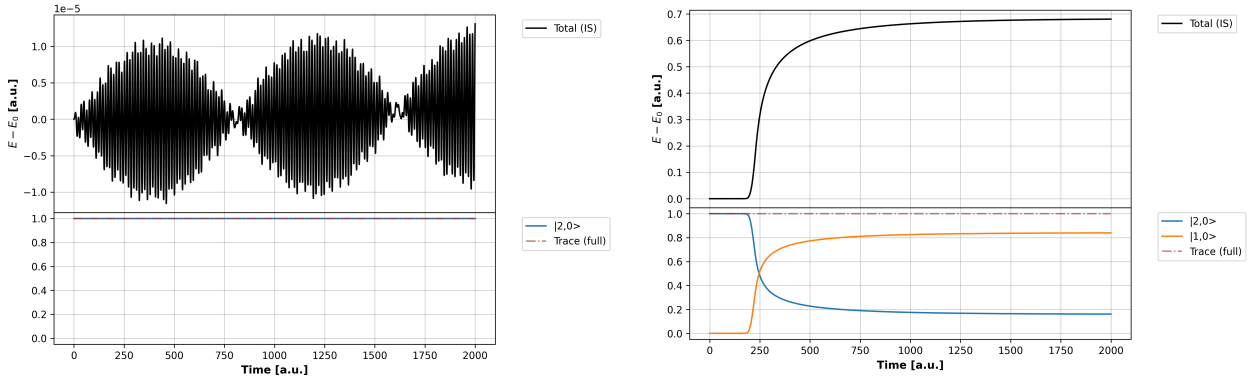

(a) **(b)**

Figure 11: Simulations of the full state, including the isospin DoF, without external fields applied for **(a)** $\Delta t = 0.01$ a.u. and **(b)** $\Delta t = 0.05$ a.u.

Finally, a simulation of the full state under the action of a magnetic field with both constant and time-varying components was performed. For this purpose, we set $\mathcal{N} = 5$, $\Delta t = 0.001$ and

$$\vec{B} = (B_1 \cos(2\pi f_r t), B_1 \sin(2\pi f_r t), B_0) \ , \tag{8}$$

with $B_0 = 119.4428$ G , $B_1 = 1.0$ G and $f_r = 1.2074958$ GHz . The choice of B_0 and f_r matches the resonance condition of the $|2,0\rangle \leftrightarrow |1,+1\rangle$ transition [29]. In addition, the geometry of the magnetic field corresponds to the so-called σ^+ polarization, which allows for a $\Delta m_F = +1$ transition. The choice of B_1 is irrelevant as long as $B_1 \lesssim 0.1 B_0$, because for $B_0 = 119.4428$ G and $\omega_r = 1.2074958$ GHz , the $|2,0\rangle \leftrightarrow |1,+1\rangle$ transition is independent of B_1 up to first order [29]. The given upper limit for B_1 assures as well that the system remains in the weak coupling regime. Increasing its value to $B_1 \simeq B_0$ would induce some state mixing as well as off-resonant transitions [30, 31], and

higher values would bring the system into a strong coupling regime, where both the adiabacity and Born-Oppenheimer approximations would not be valid anymore [32–34]. The described effects of going into the intermediate and strong coupling regimes are shown in Figs. 12a and 12b, respectively.

Unfortunately, the simulation within the weak field regime did not yield the expected results (Fig. 13). Instead, coherent oscillations of the population can be observed between the hyperfine states $|2,0\rangle$ and $|1,0\rangle$. However, these must not be mistaken for Rabi oscillations. We believe that these are so-called quantum beats. For any bias $B_0 \neq 0$, the hyperfine states are no longer eigenstates of the static hyperfine Hamiltonian, i.e., H_{HF} plus the terms from H_{Z} that involve a non-oscillating magnetic field. Instead, for bias values as large as the transition considered here, the proper eigenstates are Breit-Rabi states, which are statistical mixtures of hyperfine states [35]. An example of a transition between Rabi eigenstates for $B_0 = 119.4428$ G is the one between

$$|+,0\rangle := \cos(\theta_{\mathrm{mF=0}})\,|2,0\rangle + \sin(\theta_{\mathrm{mF=0}})\,|1,0\rangle \qquad \text{and} \qquad |\phi_0^+\rangle := \cos(\theta_{\mathrm{mF=1}})\,|1,1\rangle - \sin(\theta_{\mathrm{mF=1}})\,|2,1\rangle\ ,$$

at a frequency of $f_r \approx 6.3047541$ GHz. Thereby, θ_{mF} is the corresponding mixing angle. Therefore, if we initialize our system in the $|2,0\rangle$ hyperfine state, the strongest transition driven by our Hamiltonian, i.e., the transition with the largest matrix element will be that between $|2,0\rangle$ and $|1,0\rangle$. This is, in fact, a so-called "clock transition", because it is completely independent of the magnetic field strength at first order.

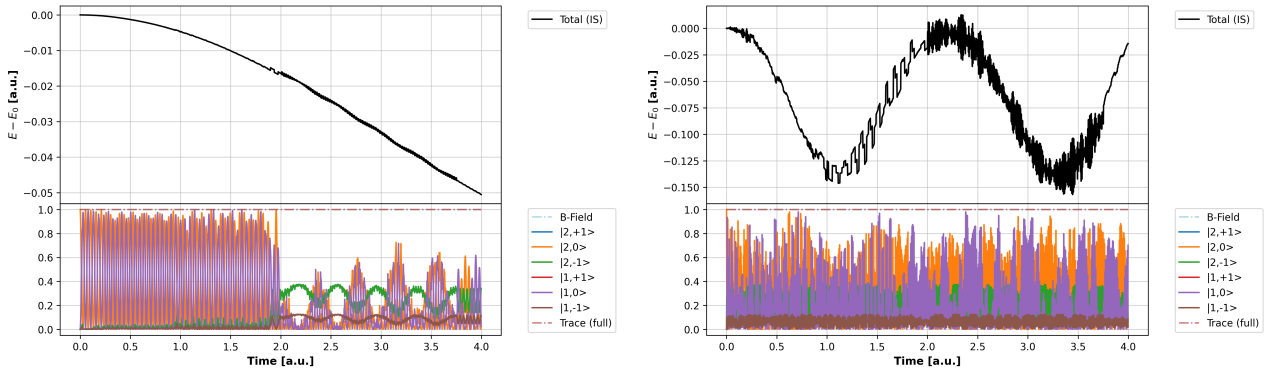

(a) **(b)**

Figure 12: Simulations of the full state, including the isospin DoF, with an external B-field as described by Eq. (8). Figure **(a)** corresponds to an intermediate field regime ($B_1 \simeq B_0$), and **(b)** to a strong field regime ($B_1 \gg B_0$).

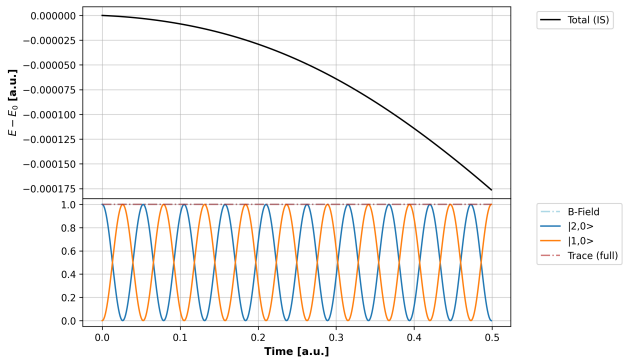

Figure 13: Simulations of the full state, including the isospin DoF, with an external B-field as described by Eq. (8) in the weak driving regime ($B_1 \lesssim 0.1 B_0$).

To observe proper Rabi oscillations between Breit-Rabi states for this type of transition is, for our understanding, very difficult. The mentioned transition at $B_0 = 119.4428$ G corresponds to a

Rabi frequency of $\Omega_R \approx 188$ kHz for a weak-driving field of $B_1 = 1$ G, or equivalently a period of $T_R \approx 5.3$ µs. In atomic units, this value is on the order of $4 \cdot 10^{10}$ a.u. As explained before, based on Fig. 11a, this type of simulation requires $\Delta t < 0.01$ a.u. to achieve energy convergence. In the upper limit of $\Delta t = 0.01$, this would imply that $\sim 4 \cdot 10^{12}$ time steps would be needed to observe a full Rabi oscillation. If one examines Fig. 14, it can be easily seen that the introduction of the isospin DoF and, in particular, of time-varying magnetic fields drastically increases the computational time per simulation step. This is mainly due to the internal implementation of the WaveBlockND package. We use this package, as explained earlier, to calculate the matrix coefficients for the evolution of the external state. This matrix depends on the magnetic field and hence must be computed at every time step for time-varying B-fields, which is very slow (on the order of $1 \sim 2$ seconds per calculation for $\mathcal{N} = 5$). This means that even a one-million-fold optimization in the computational time per simulation step would require an unfeasible amount of time.

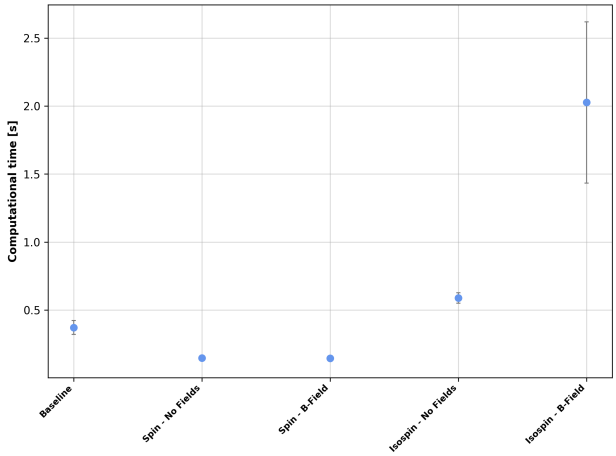

Figure 14: Computational time per simulation step for various tests. All the tests used for this plot were performed with the same cutoff value of $\mathcal{N} = 5$.

3 Conclusion

In this work, we realized an implementation based on the works of M. Solinas [4] and R. Husistein [3] that deals with the simulation of the full quantum state of a single ion under the effects of an external EM field. First, we found a data structure that allows the user to track the full state in a single matrix element despite the incompatibilities between the internal implementations of the packages used to simulate the time evolution of the electronic and external states. Then, we developed a model for the interaction between the internal and external states. We validated its implementation by comparing the results of tests performed on spin states under the effect of a magnetic field with the expected theoretical behaviors. In addition, we studied the convergence of our models in dependence on the time step duration as well as the cutoff value for the truncated Fock basis. Finally, we added the isospin DoF in the hope of being able to observe coherent Rabi oscillations. Although this last attempt was unsuccessful, we strongly believe that further investigation into the following topics could lead to a positive result:

- A completely new and optimized implementation of the methods used in the WaveBlockND package could lead to a large improvement in the computational time needed per simulation step. This could also be seen as an opportunity to develop a method that approaches the definition of the quantum state based on a single, full-state basis. If successful, a single Hamiltonian could suffice to implement the time evolution of the system.
- It is unclear, from the implementations of both the WaveBlockND and PySCF packages, what units the physical quantities are supposed to have. While we can assume, as it is for most Quantum Chemistry implementations, that PySCF works in Hartree/atomic units, our results for the dependence of the frequency of the Larmor precession on the magnetic field strength (Fig.6b) seem to hint that magnetic fields given in Tesla are interpreted as atomic units of magnetic field strength. Based on these observations, a deeper investigation than what we were able to test could reveal whether all blocks of code used in this implementation are consistent in terms of physical units.
- If the necessity of matching resonance conditions as well as of choosing the simulation parameter to achieve convergence results in a huge number of time steps per Rabi cycle, we think that a full re-scaling of the involved quantities could be studied. If such a modification would allow us to match the resonance conditions, the expected behavior of the coherent Rabi oscillations could at least be demonstrated qualitatively.

References

[1] K. A. Brown and T. Roser, "Towards storage rings as quantum computers", Physical Review Accelerators and Beams **23**, 054701 (2020).

[2] T. Schätz, U. Schramm, and D. Habs, "Crystalline ion beams", Nature **412**, 717 (2001).

[3] R. T. Husistein, *Simulation of Phonon States in Accelerators*, 2023, https://amas.pages.psi.ch/ETH/cse/Simulation_of_Phonon_States_in_Accelerators_Raphael_Husistein_V2.pdf.

[4] M. Solinas, *Extending RT-TDHF to include magnetic field interactions.* 2024, https://amas.web.psi.ch/people/aadelmann/ETH-Accel-Lecture-1/projectscompleted/phys/Semester_project_Massimo_Solinas.pdf.

[5] V. Gradinaru and G. A. Hagedorn, "Convergence of a semiclassical wavepacket based time-splitting for the Schrödinger equation", Numerische Mathematik **126**, 53 (2014).

[6] R. Heid, "Density functional perturbation theory and electron-phonon coupling", in *Correlated electrons: from models to materials*, Vol. 10, edited by E. Pavarini, E. Koch, and U. Schollwöck, NIC Series (Forschungszentrum Jülich GmbH, Institute for Advanced Simulation, 2013), pp. 217–251, https://www.cond-mat.de/events/correl13/manuscripts/heid.pdf.

[7] P. W. Atkins and R. S. Friedman, *Molecular quantum mechanics* (Oxford University Press, 2011).

[8] F. Welper, *Towards a simulation of phonon states in quantum crystalline beams.* 2024.

[9] D. Walls and G. J. Milburn, *Quantum optics* (Springer, 2025).

[10] X. Hu and F. Nori, "Quantum phonon optics: Coherent and squeezed atomic displacements", Physical Review B **53**, 2419 (1996).

[11] M. B. Plenio and P. L. Knight, "The quantum-jump approach to dissipative dynamics in quantum optics", Rev. Mod. Phys. **70**, 101 (1998) 10.1103/RevModPhys.70.101, https://link.aps.org/doi/10.1103/RevModPhys.70.101.

[12] G. Golub and C. Van Loan, *Matrix Computations*, Johns Hopkins Studies in the Mathematical Sciences (Johns Hopkins University Press, 2013), https://books.google.ch/books?id=X5YfsuCWpxMC.

[13] R. A. Horn and C. R. Johnson, *Matrix analysis* (Cambridge University Press, 2012).

[14] L. Challis, *Electron-Phonon Interactions in Low-Dimensional Structures* (Oxford University Press, 2003).

[15] P. Florków and S. Lipiński, "Impact of electron–phonon coupling on electron transport through T-shaped arrangements of quantum dots in the Kondo regime", Beilstein Journal of Nanotechnology **12**, 1209 (2021).

[16] G. D. Mahan, "Electron-Phonon Interaction", in *Many-particle physics* (Springer, 2000), pp. 433–498.

[17] H. Bruus and K. Flensberg, *Many-body quantum theory in condensed matter physics: an introduction* (Oxford University Press, 2004).

[18] M. Tinkham, *Introduction to superconductivity* (Courier Corporation, 2004).

[19] W. Domcke, H. Koppel, and D. R. Yarkony, *Conical intersections: electronic structure, dynamics & spectroscopy*, Vol. 15 (World Scientific, 2004).

[20] J. J. Sakurai and J. Napolitano, *Modern quantum mechanics* (Cambridge University Press, 2020).

[21] I. N. Levine, *Quantum Chemistry*, 7th (Pearson, New York, NY, 2014).

[22] F. Jensen, *Introduction to computational chemistry* (John Wiley & sons, 2017).

[23] J.-Q. Liao and F. Nori, "Single-photon quadratic optomechanics", Scientific reports **4**, 6302 (2014).

[24] J. Machado and Y. M. Blanter, "Quantum nonlinear dynamics of optomechanical systems in the strong-coupling regime", Physical Review A **94**, 063835 (2016).

[25] H. Yang, "Electron-Electron and Electron-Phonon Interactions in Semiconductors and Insulators from Many-Body Perturbation Theory", PhD thesis (The University of Chicago, 2021).

[26] S. Poncé and X. Gonze, "In search of the electron-phonon contribution to total energy", arXiv preprint arXiv:2512.04897 (2025).
[27] D. J. Griffiths and D. F. Schroeter, *Introduction to quantum mechanics* (Cambridge University Press, 2018).
[28] R. J. Glauber, "Coherent and incoherent states of the radiation field", Physical Review **131**, 2766 (1963).
[29] H.-Y. Lo, "Creation of squeezed Schrödinger's cat states in a mixed-species ion trap", PhD thesis (ETH Zurich, 2015).
[30] Z. Lü and H. Zheng, "Effects of counter-rotating interaction on driven tunneling dynamics: Coherent destruction of tunneling and Bloch-Siegert shift", Physical Review A—Atomic, Molecular, and Optical Physics **86**, 023831 (2012).
[31] Z. Lü, Y. Yan, H.-S. Goan, and H. Zheng, "Bias-modulated dynamics of a strongly driven two-level system", arXiv preprint arXiv:1602.04413 (2016).
[32] P Forn-Díaz, L Lamata, E Rico, J Kono, and E Solano, "Ultrastrong coupling regimes of light-matter interaction", Reviews of Modern Physics **91**, 025005 (2019).
[33] J.-F. Huang, J.-Q. Liao, and L.-M. Kuang, "Ultrastrong Jaynes-Cummings model", Physical Review A **101**, 043835 (2020).
[34] D. Burgarth, P. Facchi, R. Hillier, and M. Ligabò, "Taming the rotating wave approximation", Quantum **8**, 1262 (2024).
[35] C. J. Foot, *Atomic physics*, Vol. 7 (Oxford University Press, 2005).
[36] Z. Ficek and S. Swain, *Quantum interference and coherence: theory and experiments* (Springer, 2005).
[37] M. Tinkham, *Group theory and quantum mechanics* (Courier Corporation, 2003).
[38] M. Born and K. Huang, *Dynamical theory of crystal lattices* (Oxford University Press, 1996).
[39] C. C. Tannoudji, B. Diu, and F. Laloë, *Quantum mechanics* (John Wiley & Sons, 2020).
[40] L.-Y. Tang, J.-Y. Zhang, Z.-C. Yan, T.-Y. Shi, J. F. Babb, and J. Mitroy, "Calculations of polarizabilities and hyperpolarizabilities for the Be+ ion", Physical Review A—Atomic, Molecular, and Optical Physics **80**, 042511 (2009).
[41] J. K. Buchanan and P. G. Plieger, "9Be nuclear magnetic resonance spectroscopy trends in discrete complexes: an update", Zeitschrift für Naturforschung B **75**, 459 (2020) doi:10.1515/znb-2020-0007, https://doi.org/10.1515/znb-2020-0007.

Appendices

A Calculation of state populations

A.1 Case 1: Spin states

When considering a quantum state consisting of the electronic, phononic, and spin DoFs, the relevant populations are the spin states. For a quantum state, the internal state is often represented as a spinor,

$$|\Psi_{\text{int}}\rangle = \begin{pmatrix} |\psi_{\text{el}}\rangle \otimes |\uparrow\rangle \\ |\psi_{\text{el}}\rangle \otimes |\downarrow\rangle \end{pmatrix} =: \begin{pmatrix} |\psi^{(+)}\rangle \\ |\psi^{(-)}\rangle \end{pmatrix},$$

where $|\psi^{(+)}\rangle$ and $|\psi^{(-)}\rangle$ are known as the spin-up and spin-down states. Such states are relevant, e.g., when studying the Zeeman effect on the quantum system.

In this case, the matrix W is of shape $(2, 2, \mathcal{K}, \mathcal{K}, \mathcal{N}, \mathcal{N})$. Then, by tracing out the external state subspace, the matrix

$$R := \text{tr}_m \{W\} = \sum_m \langle m|W|m\rangle$$

can be defined, which is a block matrix of the form

$$R = \begin{pmatrix} |\psi^{(+)}\rangle\langle\psi^{(+)}| & |\psi^{(+)}\rangle\langle\psi^{(-)}| \\ |\psi^{(-)}\rangle\langle\psi^{(+)}| & |\psi^{(-)}\rangle\langle\psi^{(-)}| \end{pmatrix} =: \begin{pmatrix} R_{00} & R_{01} \\ R_{10} & R_{11} \end{pmatrix}.$$

Therefore, the populations are given by

$$\mathcal{P}\left(|\psi^{(+)}\rangle\right) = \text{tr}\{R_{00}\} \qquad \text{and} \qquad \mathcal{P}\left(|\psi^{(-)}\rangle\right) = \text{tr}\{R_{11}\}.$$

A.2 Case 2: Hyperfine states

If the isospin DoF is also considered, quantum states can be expressed on the uncoupled basis $|I, m_I; J, m_J\rangle$, where the tuple (J, m_J) refers to the electronic angular momentum and its z-projection, and the tuple (I, m_I) to the isospin and its z-projection. Alternatively, by defining $F = J + I$, the state can be represented in the so-called coupled basis

$$|F, m_F\rangle = \sum_{m_J, m_I} \langle I, m_I; J, m_J|F, m_F\rangle\, |I, m_I; J, m_J\rangle =: \sum_{m_J, m_I} \text{CG}^{(F, m_F)}_{(I, m_I; J, m_J)}\, |I, m_I; J, m_J\rangle.$$

The states $|F, m_F\rangle$ are precisely the hyperfine states, and the conversion between both bases can be achieved by means of Clebsch-Gordan (CG) coefficients.

For the particular case of $I = 3/2$ and $J = 1/2$, which is relevant for this project, the conversion between bases can be represented by a matrix

$$U_{\text{CG}} = \begin{pmatrix} 1 & 0 & 0 & 0 & 0 & 0 & 0 & 0 \\ 0 & 1/2 & 0 & 0 & 0 & \sqrt{3}/2 & 0 & 0 \\ 0 & \sqrt{3}/2 & 0 & 0 & 0 & -1/2 & 0 & 0 \\ 0 & 0 & 1/\sqrt{2} & 0 & 0 & 0 & 1/\sqrt{2} & 0 \\ 0 & 0 & 1/\sqrt{2} & 0 & 0 & 0 & -1/\sqrt{2} & 0 \\ 0 & 0 & 0 & \sqrt{3}/2 & 0 & 0 & 0 & 1/2 \\ 0 & 0 & 0 & 1/2 & 0 & 0 & 0 & -\sqrt{3}/2 \\ 0 & 0 & 0 & 0 & 1 & 0 & 0 & 0 \end{pmatrix},$$

where the columns correspond to the hyperfine states

$$|2, +2\rangle, |2, +1\rangle, |2, 0\rangle, |2, -1\rangle, |2, -2\rangle, |1, +1\rangle, |1, 0\rangle, |1, -1\rangle$$

from left to right, and the rows to the z-projections

$$|+3/2,+1/2\rangle\,,|+3/2,-1/2\rangle\,,|+1/2,+1/2\rangle\,,|+1/2,-1/2\rangle\,,$$
$$|-1/2,+1/2\rangle\,,|-1/2,-1/2\rangle\,,|-3/2,+1/2\rangle\,,|-3/2,-1/2\rangle$$

from top to bottom.

To calculate the populations in this case, one starts again by tracing out both the phononic and electronic subspaces, i.e., by defining

$$R_{\text{unc}} = \text{tr}_{k,m}\{W\}\,,$$

which yields a partial density matrix in the uncoupled isospin-spin basis. Since hyperfine states are linear combinations of these basis states, correlations must be taken into account because some of them may interfere constructively. This is particularly relevant as long as the partial density matrix in the uncoupled basis is not diagonal [20, 36]. Therefore, in order to extract the populations, the matrix R_{unc} should be transformed to the coupled basis as

$$\rho_{\text{hf}} = U_{\text{CG}}^{\dagger}\,\rho_{\text{unc}}\,U_{\text{CG}}\,,$$

where ρ_{unc} corresponds to R_{unc} reshaped into a true partial density matrix. Then, the populations are given by the diagonal elements of ρ_{unc}, where the i-th diagonal element corresponds to the hyperfine state of the i-th column label in U_{CG}.

B Calculation of the $\epsilon_{n,\eta}$ coefficients in Eq. (7)

Define

$$\mathcal{S} = \left\{\vec{\sigma} = (n_x, n_y, n_z)\,\middle|\, n_x + n_y + n_z = n\right\}$$

such that

$$|n\rangle = \sum_{\vec{\sigma}\in\mathcal{S}} \frac{1}{\sqrt{|\mathcal{S}|}}\,|\sigma\rangle\,.$$

Let

$$|n\rangle = \sum_{\vec{b}\in\mathcal{B}} \alpha_{n,\vec{b}}\,|b\rangle$$

be its projection onto HWP, where $\mathcal{B} = \{(0,0,0),\ldots,(n,n,n)\}$, and

$$\alpha_{n,\vec{b}} = \begin{cases} 1/\sqrt{|\mathcal{S}|} & \text{if } \vec{b}\in\mathcal{S} \\ 0 & \text{otherwise} \end{cases}$$

For the time evolution of $|n\rangle$, it holds after one timestep given by the operator $\hat{G}$ that

$$|n'\rangle := \hat{G}\,|n\rangle = \sum_{\vec{b}\in\mathcal{B}} \tilde{\alpha}_{n,\vec{b}}\,|b\rangle = \sum_{\eta=0}^{\mathcal{N}} \epsilon_{n,\eta}\,|\eta\rangle\,. \tag{9}$$

Note that the last equality in Eq. (9) follows because of the properties of both H_{ext} and the HWP: the operator $\hat{G}$ works as a rotation on the space spanned by $\{|0\rangle,\ldots,|\mathcal{N}\rangle\}$.

Since the $|\eta\rangle$ are Fock states, and hence orthonormal, it holds

$$\begin{aligned}\epsilon_{n,\eta} = \langle\eta|n'\rangle &= \sum_{\vec{\sigma}\in\mathcal{S}} \frac{1}{\sqrt{|\mathcal{S}|}}\,\langle\sigma|\left(\sum_{\vec{b}\in\mathcal{B}} \tilde{\alpha}_{n,\vec{b}}\,|b\rangle\right) \overset{(\star)}{=} \sum_{\vec{\sigma}\in\mathcal{S}} \frac{1}{\sqrt{|\mathcal{S}|}}\,\langle\sigma|\left(\sum_{b_x+b_y+b_z=\eta} \tilde{\alpha}_{n,\vec{b}}\,|b\rangle\right) \\ &= \sum_{\vec{\sigma}\in\mathcal{S}} \sum_{b_x+b_y+b_z=\eta} \frac{\tilde{\alpha}_{n,\vec{b}}}{\sqrt{|\mathcal{S}|}} \underbrace{\langle\sigma|b\rangle}_{:=\delta_{\sigma b}} = \sum_{b_x+b_y+b_z=\eta} \frac{\tilde{\alpha}_{n,\vec{b}}}{\sqrt{|\mathcal{S}|}}\,.\end{aligned}$$

Thereby $(\star)$, we assumed that $\tilde{\alpha}_{n,\vec{b}} = 0$ if $\vec{b}\notin\mathcal{S}$ must hold for the state to remain in the considered subspace after time evolution. Note that this assumption leads to the norm leakage phenomenon, which is then addressed as explained in Section 1.3.3.

C Calculation of the coupling strength for the nuclear displacement operator $\hat{X}$

The time evolution of a harmonic oscillator is governed by a Hamiltonian that can generically be written as $H = T + V$, i.e., as the sum of the kinetic and potential operators. For a nucleus modeled as a linear combination of harmonic oscillators, the potential can be expanded for small displacements $\vec{u} := \vec{R}_0 - \vec{R}$ around the equilibrium as

$$V(\vec{u}) \approx V_0 - \sum_\nu \frac{1}{2} k_\nu u_\nu^2 ,$$

where k_ν is the coupling strength along the direction $\nu \in \{x, y, z\}$. Therefore, it follows

$$k_\nu = \left. \frac{\partial^2 V}{\partial u_\nu^2} \right|_{\vec{u}=\vec{R}_0} . \tag{10}$$

The harmonic approximation in the expansion of the potential is adequate for small oscillations around the equilibrium. In such cases, terms of cubic order or higher, which correspond to nonlinear perturbations of the energy, are strongly suppressed with respect to the quadratic term. Those terms only become relevant for energetic perturbations that would lead to high excitation levels or even molecule dissociation. In our context, we can automatically discard those cases, since they would violate the assumptions of the Born-Oppenheimer approximation, which is inherent to our whole discussion. We chose this approach because it is often used to describe molecular vibrations as well as phonons in solids [37, 38].

A naive approach to the next step would be to assume that the restoring force is of Coulomb-type nature. In particular, this assumption would justified for short- and even intermediate-range displacements, since at such distances, quantum electrodynamic effects are much weaker [39]. Furthermore, no modifications due to core shielding effects would be required, because these are already included computationally when using ECP and Slater orbital models [21]. Then, the potential to be considered in the computation of $\vec{k}$ would be of the form

$$V(\vec{u}) = -\frac{Z_{\text{eff}} q_{\mathbf{e}}^2}{4\pi\varepsilon_0 |\vec{u}|} \approx V_0 - \frac{1}{2} \frac{Z_{\text{eff}} q_{\mathbf{e}}^2}{4\pi\epsilon_0 \langle r \rangle^3} |\vec{u}|^2 , \tag{11}$$

where $\langle r \rangle$ represents the valence shell orbital radius, and $q_{\mathbf{e}}$ the electron charge. From Eqs. (10) and (11), it would follow that

$$k_\nu \approx \frac{Z_{\text{eff}} q_{\mathbf{e}}^2}{4\pi\epsilon_0 \langle r \rangle^3} .$$

As preliminary tests demonstrate, this is barely a toy model, which yields qualitatively acceptable results but does not capture the entire effects of how the electronic cloud of the ion rearranges with the movement of the nucleus due to, e.g., polarization, exchange-correlation, or multipole effects.

A different approach is to assume that the change in the potential due to a small displacement can be described by means of the energy stored in the induced dipole of a linear-response, i.e., static polarizable electronic cloud:

$$E_{\text{ind-dip}} = \sum_\nu \frac{p_\nu^2}{2\delta_{\text{sp}}} = \sum_\nu \frac{q_{\mathbf{e}}^2 u_\nu^2}{2\delta_{\text{sp}}} ,$$

where δ_{sp} is the static dipole polarizability of the ion. Then, again by comparison with Eq. (10),

$$k_\nu \approx \frac{q_{\mathbf{e}}^2}{\delta_{\text{sp}}} .$$

Since the numerical value of δ_{sp} has been determined to high precision from very accurate correlated electronic-structure calculations based on Hylleraas and FCCI methods, it includes the electronic

many-body response that was missing in the toy model [40]. Hence, it does not only include all the assumptions made in the description the previous approach, but is also more complete.

With this, the angular frequency of the nucleus along ν of the oscillations generated by this potential is

$$\omega_\nu = \sqrt{\frac{k_\nu}{M}}\,,$$

where M is the mass of the nucleus. Finally, the prefactor or coupling strength for the nuclear operator along ν is computed as

$$g_\nu := \frac{\hbar\omega_\nu}{4}\,.$$

Quantity	**Value**	**Reference**
δ_{sp}	$24.4966 \cdot 4\pi\varepsilon_0 a_0^3$	[40]
M	9.012183050 amu	[41]

Table 1: Numerical values and references for the quantities used in the estimation of k_ν , ω_ν and g_ν for the ground state $^9\text{Be}^+$ ion. Thereby, a_0 is the Bohr radius.

Estimation of g_ν for the $^9\text{Be}^+$ ion

For the $^9\text{Be}^+$ ion in the ground state, the valence electron lies in the 2s orbital. For our calculations, we use the values given in Table 1. Then, we have in SI units[13]

$$k_{\nu,\,\text{SI}} \approx \frac{\left(1.602176634 \cdot 10^{-19}\right)^2}{4\pi \cdot 8.854187817 \cdot 10^{-12} \cdot 24.4966 \cdot \left(5.29177109 \cdot 10^{-11}\right)^3} = 63.55547717260995 \text{ N/m}\,,$$

$$\omega_{\nu,\,\text{SI}} = \sqrt{\frac{k_\nu}{M}} \approx \sqrt{\frac{63.55547717260995}{9.012183050 \cdot 1.66054 \cdot 10^{-27}}} = 6.5116838238011957 \cdot 10^{14} \text{ rad/s}\,,$$

$$g_{\nu,\,\text{SI}} = \sqrt{\frac{\hbar}{2M\omega_\nu}} \approx \sqrt{\frac{1.054571817 \cdot 10^{-34}}{2 \cdot 9.012183050 \cdot 1.66054 \cdot 10^{-27} \cdot 6.5116838238011957 \cdot 10^{14}}} = 1.718118485438837 \cdot 10^{-21} \text{ J}\,.$$

Considering now the conversion factor for energy from SI to atomic units (a.u.),

$$J_{\text{a.u.}} = 4.3597447222071 \cdot 10^{-18} \text{ J}\,,$$

we obtain

$$g_{\nu,\,\text{a.u.}} \approx 1.718118485438837 \cdot 10^{-21} \cdot \frac{1}{J_{\text{a.u.}}} = 3.9400869465790758 \cdot 10^{-4} \text{ a.u.}\,.$$

[13] Note that in the discussion above, g_ν did not have a $\hbar$ factor. This is because in our simulations, we use atomic units with $\hbar = 1$, but this factor is needed for the numerical computation in SI units.

Eidgenössische Technische Hochschule Zürich
Swiss Federal Institute of Technology Zurich

Declaration of Originality

The signed declaration of originality is a component of every semester paper, Bachelor's thesis, Master's thesis and any other degree paper undertaken during the course of studies, including the respective electronic versions.

Lecturers may also require a declaration of originality for other written papers compiled for their courses.

I hereby confirm that I am the sole author of the written work here enclosed and that I have compiled it in my own words. Parts excepted are corrections of form and content by the supervisor.

Title of Master's thesis (in block letters):

Authored by (in block letters):
For papers written by groups the names of all authors are required.

Name(s):	**First name(s):**

With my signature I confirm that

- I have committed none of the forms of plagiarism described in the 'Citation etiquette' information sheet.
- I have documented all methods, data and processes truthfully.
- I have not manipulated any data.
- I have mentioned all persons who were significant facilitators of the work.

I am aware that the work may be screened electronically for plagiarism.

Place, date	**Signature(s)**
	

For papers written by groups the names of all authors are required. Their signatures collectively guarantee the entire content of the written paper.